



## Electrospinning of Polyvinylidene Fluoride Membranes: Effect of Membrane Composition and Fabrication Conditions

Zeyad Zeitoun <sup>[a]</sup>, Ahmed H. El-Shazly <sup>[a,b]</sup>, Shaaban Nosier <sup>[a]</sup>, Mohamed R. Elmarghany <sup>[c,d]</sup>, Mohamed S. Salem <sup>[c]</sup>, Mahmoud M. Taha <sup>[a,e]</sup>



CrossMark

<sup>[a]</sup> Chemical Engineering Department, Faculty of Engineering, Alexandria University, Alexandria, Egypt

<sup>[b]</sup> Chemical and Petrochemical Engineering Department, Egypt-Japan University of Science and Technology (E-Just), Egypt

<sup>[c]</sup> Mechanical Power Engineering Department, Faculty of Engineering, Mansoura University, Egypt

<sup>[d]</sup> Director of Mansoura University Nanotechnology Center, Mansoura University, Egypt

<sup>[e]</sup> University of Science and Technology, Environmental Engineering Department, Zewail City of Science and Technology, October Gardens, Giza, Egypt.

### Abstract

Membrane fabrication by the electrospinning can provide tenable structure membranes with interconnected pores, large surface area, and high porosity. This study focuses on studying the effect of different membrane compositions (i.e., polymer concentration and inorganic additives) and electrospinning conditions (i.e., internal needle diameter, tip to collector distance, and feed flow rate) on the characteristics of polyvinylidene fluoride (PVDF) flat sheet membrane. A homogeneous dope solution was prepared by dissolving the PVDF in a mixture of dimethylacetamide (DMAc) and acetone. The electrospinning conditions producing uniform homogeneous beaded fibers are as follows: 16 wt% polymer concentration, 0.004 wt% LiCl concentration, 0.51 mm internal needle diameter, 15 cm tip to collector distance, feed flow rate of 1 ml/hr. Further analysis was conducted by using Fourier Transform Infrared Spectrometer (FTIR) and X-Ray Diffraction (XRD) to assess the impact of electrospinning on fibers elemental composition. Additionally, static water contact angle, porosity, fiber diameter, and pore size measurements reveal the formation of submicron hydrophobic fibers with random alignment.

**Keywords:** PVDF Membrane; Electrospinning; Scanning electron microscope (SEM); Fourier Transform Infrared Spectrometer (FTIR); X-Ray Diffraction (XRD).

### Introduction

Membranes are selective barriers or interphases between two bulk phases that have been widely adopted over the last 30 years for various applications such as wastewater treatment, bioreactors, gas separation, etc. [1-3]. Membranes can be fabricated from organic or inorganic materials such as polymers (i.e., cellulose acetate, polyethylene, etc.) [4], metals (i.e., stainless steel, tungsten, etc.) [5], and ceramics (i.e., a mixture of metals such as aluminum or titanium and nonmetals such as oxides, nitrides, or carbides) [5]. Each category has its characteristics and advantages that match with certain purposes and/or applications. In terms of membrane fabrication by organic materials, numerous studies in the open literature have demonstrated that the polyvinylidene

fluoride (PVDF) is a privileged choice owing to its remarkable physicochemical properties and its capabilities to fulfill predefined manufacturing requirements [4].

Several methods can be utilized for membranes' fabrication such as electrospinning, phase inversion, dip coating, etc [6-8]. Among these methods, the electrospinning has proven its high capabilities in fabricating highly porous fibrous membranes with large surface area and consistent size distribution [9]. Electrospinning is a simple technique used to fabricate submicron fibrous (i.e., fiber diameters range between micrometers and nanometers) membranes by subjecting a polymer solution to an intense electric field at a certain voltage value [10]. This critical voltage is defined as the value at which the repulsive

\*Corresponding author e-mail: [zeyad.zeitoun@alexu.edu.eg](mailto:zeyad.zeitoun@alexu.edu.eg); (Zeyad.Zeitoun).

Receive Date: 07 June 2021, Revise Date: 09 August 2021, Accept Date: 28 August 2021

DOI: 10.21608/EJCHEM.2021.77967.3913

©2022 National Information and Documentation Center (NIDOC)

electric force overcomes the solution surface tension so the solution can eject from the tip to the collector. During flowing to the collector, solidification occurs to the solution jet, due to the evaporation of the solvent, and fibers are deposited on a flat plate collector [10]. The resulting fibers are named “electrospun or e-spun fibers” and they are characterized by outstanding properties such as high porosity (may reach more than 80%) with a wide range of pore size distribution, diameters range between micrometers and nanometers with a consistent size distribution, exceptional pore interconnectivity, and high surface-to-volume ratio [11]. Therefore, different polymers (i.e., synthetic and natural polymers) have been electrospun and utilized in different applications such as filtration, conducting

devices, wound dressing, water/wastewater treatment, and scaffolds for tissue engineering [10].

While the concepts of electrospinning may seem simple on the surface, many parameters can affect the size, morphology, alignment, and quality of the fibers produced, each with a varying impact on the final product [12]. These parameters are classified as solution properties, process parameters, and environmental conditions as listed in **Error! Reference source not found.** This study is set out to delineate the membrane compositions and the electrospinning system (NANON-01A, MECC CO., LTD. JAPAN) processing conditions to fabricate a beads-free **PVDF** flat sheet membrane with uniform fiber distribution and homogeneity [13].

Table 1. Different parameters affecting the electrospinning process [9]

Solution properties	Process parameters	Environmental conditions
Concentration Viscosity Surface tension Conductivity Dielectric constant Solvent volatility	Electrostatic potential Electric field strength Electrostatic field shape Working distance Feed rate Orifice diameter	Temperature Humidity Local atmospheric flow Atmospheric composition Pressure

## Materials and methods

### Materials

Raw **PVDF** pellets ( $\rho = 1.78 \text{ g/cm}^3$ , average Mw  $\sim 275,000 \text{ g/mol}$ ), supplied from Sigma Aldrich, USA. N, N-dimethylacetamide (**DMAC**) (ACS, >99% and density of  $0.937 \text{ g/ml}$ ) and acetone (HPLC grade, > 99.9%) were purchased from DOP ORGANIK KIMYA (Turkey). Lithium chloride (**LiCl**) as an inorganic additive was purchased from Merck, Singapore.

### Membrane fabrication

#### Preparation of electrospinning dope solution

Dope solutions for electrospinning were prepared by dissolving the given amount of **PVDF** in a solvent mixture of 20 vol% **DMAC** and 80 vol% acetone as shown in **Error! Reference source not found.** Lithium chloride (**LiCl**) was added to some dope solutions to investigate the effect of inorganic additives on fibers' homogeneity. All dope solutions were subjected to continuous stirring for 12 hours at 500 rpm and  $80^\circ\text{C}$  to get a homogenous solution suitable for the electrospinning process. Then, ultrasonic degassing (LABSONIC, model: LBS2 4.5

Lt, FALC INSTRUMENTS TREVIGLIO, ITALY) was executed for 1 hour at room temperature ( $25 \pm 2^\circ\text{C}$ ) as final step before the electrospinning.

Table 2. Amount of **PVDF** and additive in the membrane samples

Dope code	Dope solution composition		
	<b>PVDF</b> (wt%)	Solvent	Additive +
E1	14 %	86 %	NA
E2	14 %	86 %	<b>LiCl</b>
E3	16 %	84 %	<b>LiCl</b>

+Percentage of **LiCl** is 0.004 wt% of the **PVDF** and solvent mixture [14]

### Electrospinning process

Electrospinning was performed in the nanofiber electrospinning system (NANON-01A, MECC CO., LTD. JAPAN, shown in **Error! Reference source not found.**). The setup consists of a horizontal syringe, capillary pump, flat plate collector, and high-power supply voltage. Throughout the experiments, some parameters were kept constant as the spinneret speed 100 mm/s, cleaning frequency 1 hr, cleaning interval 1 s, and electric voltage 20 kV. All dope solutions were electrospun for 5 hours, then the

prepared membranes were put in an oven at 60°C for 24 hours to remove the residuals of the solvents.

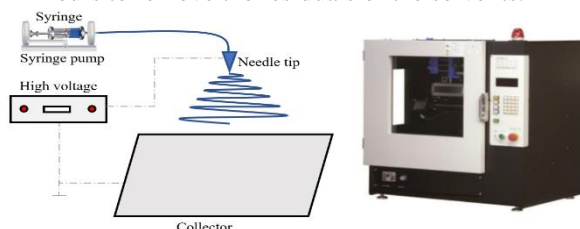


Figure 1. Electrospinning equipment and mechanism

### Membrane characterization

The PVDF electrospun membrane samples were cut into 2 cm x 2 cm flat sheet, sputtered by gold, and examined by Scanning Electron Microscope (SEM) (JEOL JSM-6010LV) to examine the morphology of the PVDF fabricated membrane and to explore the membrane composition and electrospinning conditions adequate to produce beadless fibrous membrane. More insights of the characteristics of these beadless PVDF membranes were gained by using

the Fourier Transform Infrared Spectrometer (FTIR) (Bruker Vertex 70) and X-Ray Diffraction (XRD) (Shimadzu XRD-6100) techniques and the static water contact angle (Theta Lite, Biolin Scientific, Sweden), porosity, fiber diameter, and pore size measurements. The FTIR and the XRD were used to determine the phases existing after the electrospinning process while the remaining measurements were used to evaluate membrane hydrophobicity and fibers' random alignment.

### Variables studied

In the current study, the effects of different electrospinning parameters (i.e., needle internal diameter, tip to collector distance (TCD), and pumping flow rate) as well as varying membrane composition (i.e., inorganic additives and polymer concentration), on PVDF fibrous membranes' fabrication were investigated. The examined variables are listed in **Error! Reference source not found.**

Table 3. Investigated electrospinning conditions and membrane compositions

Sample code	Flow rate (ml/hr)	Internal needle diameter (mm)	Electric voltage (kV)	Tip to collector distance (cm)	Dope code (Error! Reference source not found.)
<b>Electrospinning processing conditions</b>					
Needle internal diameters					
M1	0.5	0.26	20	13	E1
M2		0.51			
M3		0.84			
Tip to collector distances					
M4	0.5	0.51	20	11	E1
M2				13	
M5				15	
Flow rates					
M5	0.5	0.51	20	15	E1
M6	1				
M7	1.5				
M8	2.5				
<b>Membrane composition</b>					
Inorganic additive concentrations					
M7	1.5	0.51	20	15	E1
M9					E2
Polymer concentrations					
M9	1.5	0.51	20	15	E2
M10					E3

## Results and discussion

### Electrospinning processing conditions

#### Effect of internal needle diameter

As listed in **Error! Reference source not found.**, three different internal needle diameters (samples coded M1, M2, and M3) were considered namely: 0.26 mm, 0.51 mm, 0.84 mm, respectively. By

referring to Figure 2, a medium needle diameter (0.51 mm) produces a membrane with a small number of beads compared with the other values. Large needle diameter produces thick fibers that with prolonged exposure to the atmosphere could lead to clogging of the needle. On the other hand, very small needle diameters produce small diameter electrospun fibers with high surface tension forces. Therefore, greater columbic forces are required for stretching and extruding a droplet at the needle tip. Since the voltage supplied is kept constant throughout the experiments, the polymer solution is ejected as a droplet rather than fibers in case of very small diameter and a large number of beads are formed within the membrane structure [15]. Therefore, a needle with an internal diameter of 0.51 mm is more preferable than other values examined and hence used in subsequent experiments (see **Error! Reference source not found.**).

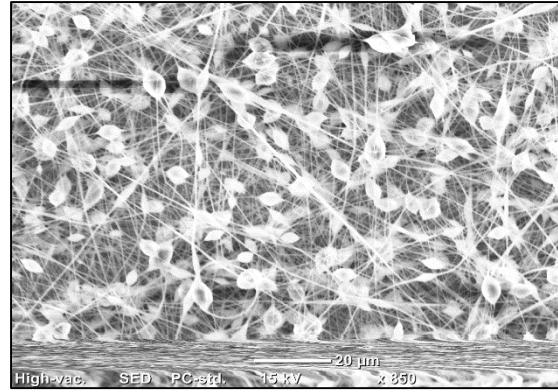
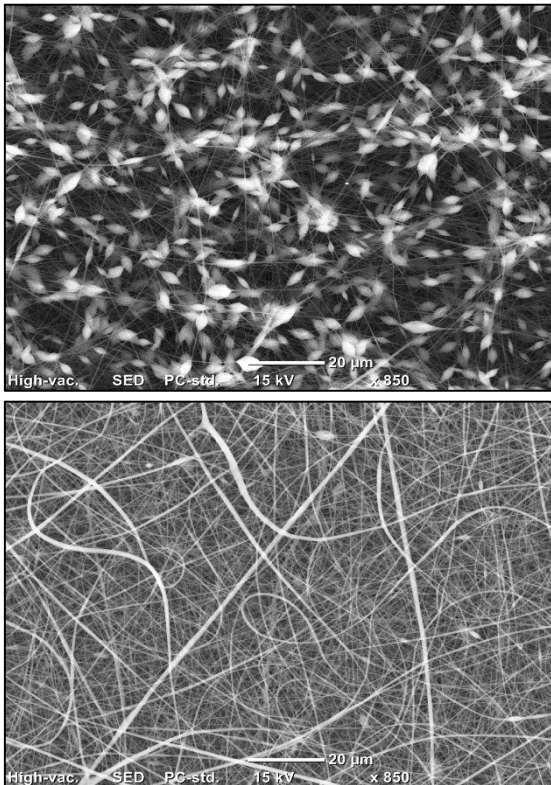


Figure 2. SEM images for (a) M1, internal needle diameter 0.26 mm; (b) M2, internal needle diameter 0.51 mm; and (c) M3, internal needle diameter 0.84 mm. Effect of tip to collector distance

The effect of the tip to collector distance (TCD) on fiber production was investigated at different values namely: 11, 13, and 15 cm for M4, M2, and M5, respectively. As shown in Figure 3, the optimum value for TCD is 15 cm. At TCD less than 15 cm, SEM results show formation of beads as shown in Figure 3. Beads formation is attributed to the short distance and subsequently the increased electric field between the tip and the collector that accelerates fibers jet travel towards the collector. This acceleration causes insufficiency of the allowable time for stretching fibers and solvent evaporation. Hence, fibers merge and form junctions on the collector. Therefore, 15 cm was selected as the optimum value for the subsequent electrospinning experiments [11].

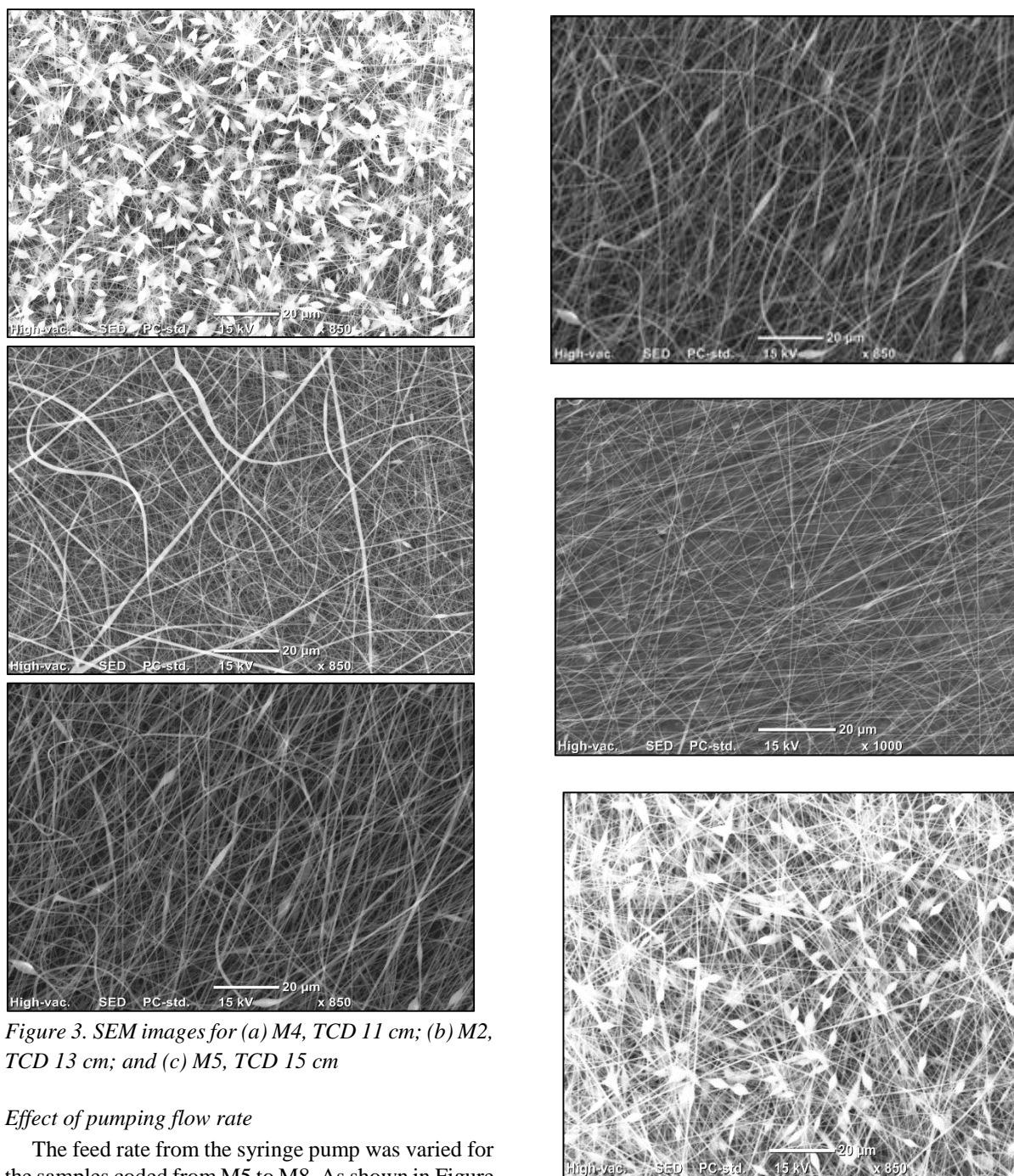


Figure 3. SEM images for (a) M4, TCD 11 cm; (b) M2, TCD 13 cm; and (c) M5, TCD 15 cm

#### Effect of pumping flow rate

The feed rate from the syringe pump was varied for the samples coded from M5 to M8. As shown in Figure 4, M6, at a feed flow rate of 1 ml/hr, has minimum beads in comparison to the other samples. Indeed, higher feed rates result in pumping large volumes of the polymer solution within insufficient time through the tip. Similarly to the low TCD values, time insufficiency causes incomplete solvent evaporation and thus fibers are allowed to fuse and causes formation of beads in the membrane structure [15, 16].

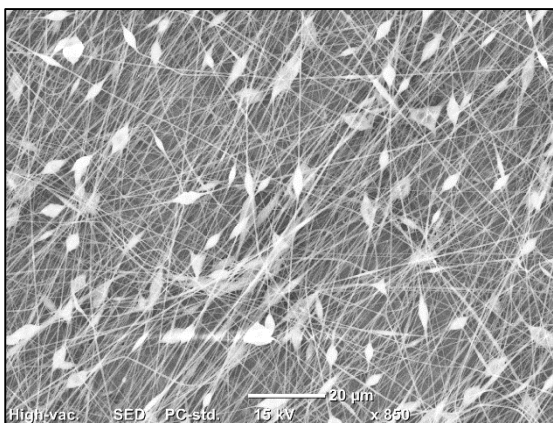


Figure 4. SEM images for: (a) M5, flow rate 0.5 ml/hr; (b) M6, flow rate 1 ml/hr; (c) M7, flow rate 1.5 ml/hr; and (d) M8, flow rate 2.5 ml/hr

#### Membrane composition

The composition of the dope solution significantly affects the membrane structure and the electrospinning process.

#### Effect of inorganic additives

The effect of *LiCl* was studied on two samples (M7 and M9) in which M9 contains 0.004 wt% of *LiCl*. As shown in Figure 5, M9 sample is characterized by more uniform electrospun fibers with fewer beads. This may be attributed to the presence of *LiCl* which improve the electrostatic interaction between *DMAc*/Acetone mixture and *PVDF* polymer leading to the enhancement of polymer solution conductivity. Increasing polymer conductivity generates a high charge density at the tip due to large self-repulsion existing between charged tip surface and negatively charged chloride ions. Moreover, large elongation forces are created due to the high mobility of these chloride ions lead to fast ejection of thin tense fibers. Accordingly, it is concluded that the *LiCl* improved the electrospun fibers structure [14].

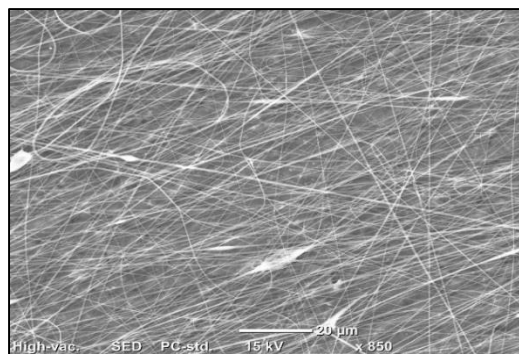
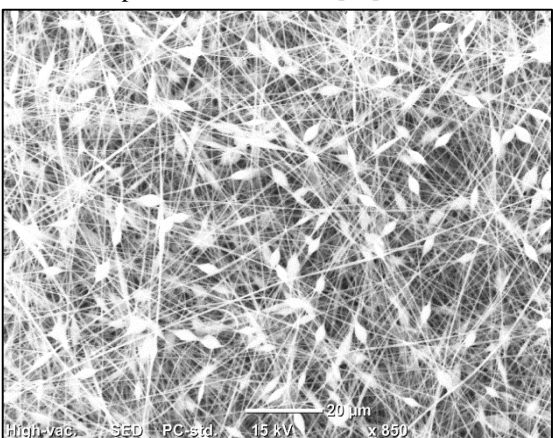


Figure 5. SEM images for (a) M7, without *LiCl* and (b) M9, with 0.004 wt% *LiCl*

#### Effect of polymer concentration

Polymer concentration significantly affects the dope solution viscosity. Increasing viscosity has contrary effects. Although high viscosity leads to the production of improved-quality fibers, exceeding certain limits would cause difficulty in pumping the dope solution through the needle. In this study, the effect of two different *PVDF* concentrations (i.e., 14 wt% and 16 wt% *PVDF* in M9 and M10, respectively) was investigated. As shown in Figure 6, M10 has shown few beads within the membrane structure due to the greater chain entanglements induced by polymer that maintain the continuity of the jet during the electrospinning [15].

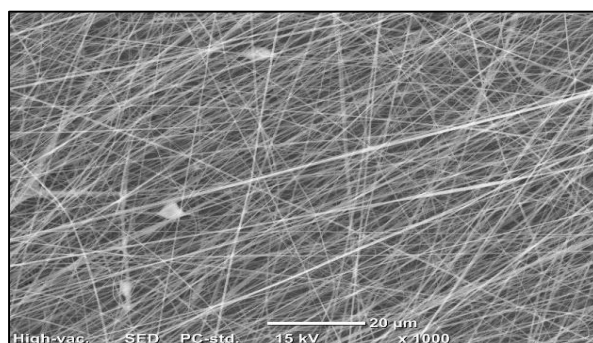
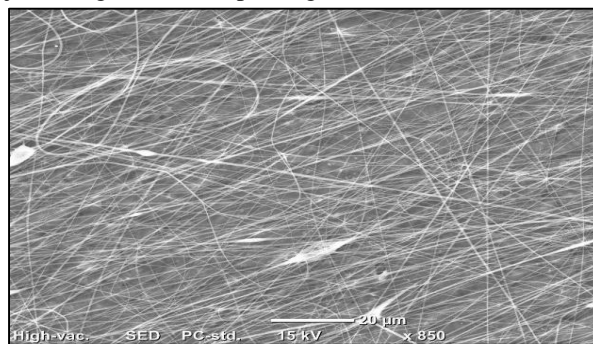


Figure 6. SEM images for (a) M9, polymer

concentration 14 wt% and (b) M10, polymer concentration 16 wt%.

Based on the previous narrative and within the present range of investigated parameters, the optimum conditions for the electrospinning system (NANON-01A, MECC CO., LTD. JAPAN) are listed in Error! Reference source not found..

Table 4. Optimum conditions for fabrication PVDF membrane

Electric voltage	20 kV
Spinneret speed	100 mm/s
Cleaning frequency	1 hr
Cleaning interval	1 s
Polymer concentration	16 wt%
Pumping flow rate	1 ml/hr
Tip to collector distance	15 cm
Internal needle diameter	0.51 mm
LiCl concentration	0.004 wt%

#### SEM characterization of optimized electrospinning process

Figure 7 shows a SEM characterization of the electrospun membrane fabricated at the conditions, mentioned in Error! Reference source not found.. It is revealed that adopting these conditions yields free beads homogenous fibers throughout the membrane structure.

Figure 7. SEM image at the optimum electrospinning conditions

#### Extensive characterization of the free beads fabricated membrane

Further characterization of the free beads PVDF membrane fabricated at the conditions mentioned in Error! Reference source not found. were conducted and discussed in the subsequent sections.

#### X-Ray Diffraction (XRD)

It is generally known that PVDF exhibit one of the following three crystalline structures, depending on the preparation conditions: Form I ( $\beta$ -type crystal with planar zigzag conformation, orthorhombic), Form II ( $\alpha$ -type crystal with TGT $\check{C}$ , monoclinic), and Form III ( $\gamma$ -type crystal with TTTGTTT $\check{C}$ , Monoclinic) [17]. Error! Reference source not found., shows the XRD

patterns for raw PVDF and electrospun PVDF membrane. For the raw PVDF, three considerable peaks are observed at  $17.58^\circ$ ,  $18.40^\circ$ , and  $20.25^\circ$ . The diffraction peaks at  $17.58^\circ$  and  $18.40^\circ$  reveal the presence of Form II ( $\alpha$ -type) which are assigned to the lattice planes (1 0 0) and (0 2 0), respectively, while the peak ( $20.25^\circ$ ) shows the presence of Form III ( $\gamma$ -type) for plane (1 0 1). The shorter apexes and wider range peaks observed for the electrospun PVDF membrane reflect a decrease in percentage crystallinity due to electrospinning. Analogous to the XRD patterns for raw PVDF, diffraction peaks, that were detected at  $17.8^\circ$  and  $19.58^\circ$ , reveal the existence of Form II ( $\alpha$ -type) and Form III ( $\gamma$ -type), respectively. [17-26]. This is consistent with the findings of [17] in which the dope solution, consists of PVDF and DMAc/Acetone mixture. It is worth to mention that both studies formed the polymer solution at temperatures higher than  $70^\circ\text{C}$  below which the  $\beta$  phase is formed [27].

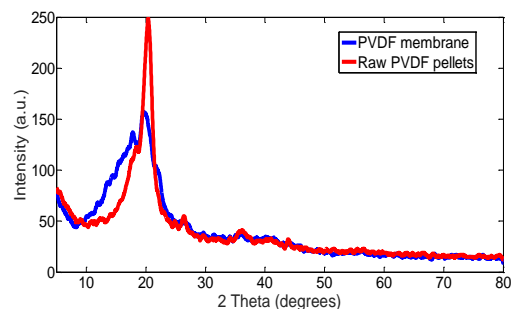
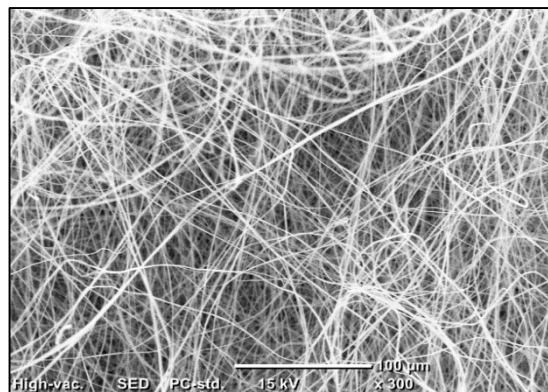


Figure 8. XRD Patterns for PVDF membrane and raw



PVDF pellets

#### Fourier Transform Infrared Spectrometer (FTIR)

The FTIR analysis shows the active bonds and phases in the membrane structure. As shown in Error! Reference source not found., peaks at  $3022$  and  $2978\text{ cm}^{-1}$  reveals the  $\text{CH}_2$  asymmetric and

symmetric stretching vibration, respectively. The peaks at  $1401$  and  $838\text{ cm}^{-1}$  show  $\text{CH}_2$  deformation and rocking vibrations, respectively, while that at  $1070\text{ cm}^{-1}$  is assigned to  $\text{C}-\text{F}$  wagging vibration. Moreover, characteristic bands at  $1174$ ,  $877$ , and  $761\text{ cm}^{-1}$  belongs to  $\text{CF}_2$  stretching, deformation, and bending vibrations, respectively. The *PVDF* membrane is also characterized by the presence of  $\alpha$ -phase at  $610\text{ cm}^{-1}$  and existence of  $\gamma$ -phase at  $1275$  and  $482\text{ cm}^{-1}$  which confirms the XRD findings mentioned above [28, 29].

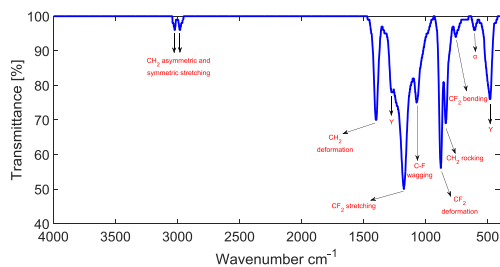


Figure 9. FTIR curve for *PVDF* membrane

#### Static water contact angle measurement

Hydrophobicity and wettability of the *PVDF* membrane can be analyzed by measuring the static water contact angle test (Theta Lite, Biolin Scientific, Sweden). This test was carried out by dropping a water droplet on the membrane surface. A high precision camera is used to capture the droplet image to be analyzed by an image software to determine the contact angle (the angle between the solid surface and the tangent to the curved surface of the drop (see **Error! Reference source not found.**)). It is observed that the water contact angle is  $130^\circ$ . Since there is an inverse proportionality between the contact value and the surface wettability, this obtained value reveals the hydrophobicity of the *PVDF* membrane.

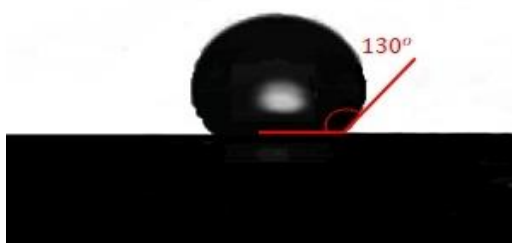


Figure 10: Static water droplet contact angle.

#### Porosity

Membrane porosity is defined as the volumetric fraction of the membrane pores. It was measured

using the gravimetric method in which membrane samples ( $3\text{ cm} \times 3\text{ cm}$ ) were fully wetted with ethanol for  $30\text{ mins}$  and then equation (1) was used to calculate the percent membrane porosity  $Ak$  [30].

$$Ak = \frac{\frac{(w_1 - w_2)}{\rho_{ethanol}}}{\frac{(w_1 - w_2)}{\rho_{ethanol}} + \frac{w_2}{\rho_{PVDF}}} \times 100 \quad (1)$$

Where  $w_1$  and  $w_2$  are the weights of the wet and dry membrane (grams), respectively,  $\rho_{ethanol}$  and  $\rho_{PVDF}$  are the specific gravities of the ethanol ( $0.789\text{ g/cm}^3$ ) and *PVDF* polymer ( $1.78\text{ g/cm}^3$ ) [30]. It is worth mentioning that, this test was repeated three times to ensure the reproducibility of the results and by substituting in equation (1), it was found that it is equal to  $90 \pm 2.1\%$ .

#### Fiber diameter and pore diameter

The average fiber diameter and pore size distribution was quantified by processing the obtained SEM images by an image processing software (ImageJ) [31]. Obtained results reveal the existence of approximately 200 pores within the membrane structure with an average pore diameter and fiber diameter of  $0.501 \pm 0.04\ \mu\text{m}$  and  $0.363 \pm 0.06\ \mu\text{m}$ , respectively. These values are in a good agreement with a previous related study for the authors [32].

#### Applications of studied *PVDF* membrane

The fabricated *PVDF* membrane at the optimum conditions is further used in wastewater treatment and water desalination to examine its performance in our lab. Firstly, it is combined with a photocatalytic reactor for methylene blue degradation [6]. Secondly, graphene oxide is added to the membrane for water desalination by direct contact membrane distillation [33].

#### Remarks and conclusion

Fibrous *PVDF* membranes were fabricated by electrospinning technique (NANON-01A, MECC CO., LTD. JAPAN) at different electrospinning processing conditions (i.e., syringe needle internal diameters, feed flow rates, tip to collector distances) and membrane compositions (i.e., inorganic additives, and polymer concentrations). The key findings are summarized as follows:

Temperature at which dope solution is formed influences the existing phases.

Inorganic additives (i.e., *LiCl*) have a positive effect on membrane structure.

The conditions determined to produce free beads homogenous fibers throughout the membrane structure are as follows: electric voltage  $20\text{ kV}$ , spinneret speed  $100\text{ mm/s}$ , cleaning frequency  $1\text{ hr}$ , cleaning interval  $1\text{ s}$ , polymer concentration  $16\text{ wt\%}$ , pumping flow rate  $1\text{ ml/hr}$ , tip to collector

distance 15 cm, internal needle diameter 0.51 mm, and LiCl concentration 0.004 wt%.

### Conflict of interest

There is no conflict of interest

### Nomenclature

#### Symbols

$A$	Membrane area ( $m^2$ )
$Ak$	Percentage porosity (%)
$Mw$	Molecular weight ( $g/mol$ )
$w_1$	Weight of wet membrane ( $grams$ )
$w_2$	Weight of dry membrane ( $grams$ )

#### Greek letters

$\beta$	Form I of PVDF crystal structure
$\alpha$	Form II of PVDF crystal structure
$\gamma$	Form III of PVDF crystal structure
$\rho_{ethanol}$	Ethanol density ( $g/cm^3$ )
$\rho_{PVDF}$	PVDF density ( $g/cm^3$ )

#### Abbreviations

<i>DMAC</i>	N-Dimethyl Acetamide
<i>FTIR</i>	Fourier Transform Infrared Spectrometer
<i>LiCl</i>	Lithium Chloride
<i>PVDF</i>	Poly-Vinylidene Flouride
<i>TCD</i>	Tip to Collector Distance
<i>TiO<sub>2</sub></i>	Titanium Dioxide
<i>XRD</i>	X-Ray Diffraction

#### Literature cited

- [1] S. Judd, The status of membrane bioreactor technology, *Trends in biotechnology* 26(2) (2008) 109-116.
- [2] P. Gabrielli, M. Gazzani, M. Mazzotti, On the optimal design of membrane-based gas separation processes, *Journal of Membrane Science* 526 (2017) 118-130.
- [3] L. Paredes, S. Murgolo, H. Dzinun, M.H.D. Othman, A.F. Ismail, M. Carballa, G. Mascolo, Application of immobilized TiO<sub>2</sub> on PVDF dual layer hollow fibre membrane to improve the photocatalytic removal of pharmaceuticals in different water matrices, *Applied Catalysis B: Environmental* 240 (2019) 9-18.
- [4] I. Ali, O. Bamaga, L. Gzara, M. Bassyouni, M. Abdel-Aziz, M. Soliman, E. Drioli, M. Albeirutty, Assessment of blend PVDF membranes, and the effect of polymer concentration and blend composition, *Membranes* 8(1) (2018) 13.
- [5] B. Ladewig, M.N.Z. Al-Shaeli, *Fundamentals of membrane bioreactors*, Springer Transactions in Civil and Environmental Engineering (2017).
- [6] Z. Zeitoun, A.H. El-Shazly, S. Nosier, M.R. Elmarghany, M.S. Salem, M.M. Taha, Performance Evaluation and Kinetic Analysis of Photocatalytic Membrane Reactor in Wastewater Treatment, *Membranes* 10(10) (2020) 276.
- [7] K. Fischer, M. Grimm, J. Meyers, C. Dietrich, R. Gläser, A. Schulze, Photoactive microfiltration membranes via directed synthesis of TiO<sub>2</sub> nanoparticles on the polymer surface for removal of drugs from water, *Journal of Membrane Science* 478 (2015) 49-57.
- [8] J. Cheng, H. Pu, A facile method to prepare polyvinylidene fluoride composite nanofibers with high photocatalytic activity via nanolayer coextrusion, *European Polymer Journal* 99 (2018) 361-367.
- [9] F.E. Ahmed, B.S. Lalia, R. Hashaikeh, A review on electrospinning for membrane fabrication: challenges and applications, *Desalination* 356 (2015) 15-30.
- [10] J.-S. Park, Electrospinning and its applications, *Advances in Natural Sciences: Nanoscience and Nanotechnology* 1(4) (2011) 043002.
- [11] L. Zaidouny, M. Abou- Daher, A.R. Tehrani-Bagha, K. Ghali, N. Ghaddar, Electrospun nanofibrous polyvinylidene fluoride-co-hexafluoropropylene membranes for oil-water separation, *Journal of Applied Polymer Science* 137(34) (2020) 49394.
- [12] J.W. Rajala, *Electrospinning Fabrication of Ceramic Fibers for Transparent Conducting and Hollow Tube Membrane Applications*, University of Akron, 2016.
- [13] J. Stanger, N. Tucker, A. Wallace, N. Larsen, M. Staiger, R. Reeves, The effect of electrode configuration and substrate material on the mass deposition rate of electrospinning, *Journal of applied polymer science* 112(3) (2009) 1729-1737.
- [14] Y. Liao, R. Wang, M. Tian, C. Qiu, A.G. Fane, Fabrication of polyvinylidene fluoride (PVDF) nanofiber membranes by electro-spinning for direct contact membrane distillation, *Journal of Membrane Science* 425 (2013) 30-39.
- [15] S. Ramakrishna, *An introduction to electrospinning and nanofibers*, World Scientific 2005.
- [16] S. Tabe, A Review of Electrospun Nanofiber Membranes, *Journal of Membrane Science and Research* 3(3) (2017) 228-239.
- [17] S.W. Choi, J.R. Kim, Y.R. Ahn, S.M. Jo, E.J. Cairns, Characterization of electrospun PVDF fiber-based polymer electrolytes, *Chemistry of materials* 19(1) (2007) 104-115.

- [18] Y. Chen, J. Guo, H. Kim, Preparation of poly (vinylidene fluoride)/phosphotungstic acid composite nanofiber membranes by electrospinning for proton conductivity, *Reactive and Functional Polymers* 70(1) (2010) 69-74.
- [19] S.A. Salman, F.T. Noori, A.K. Mohammed, Preparation and Characterizations of Poly (vinylidene fluoride)(PVDF)/Ba<sub>0.6</sub>Sr<sub>0.4</sub>TiO<sub>3</sub> (BST) Nanocomposites, *International Journal of Applied Engineering Research* 13(7) (2018) 5008-5013.
- [20] A.K. Zak, W.C. Gan, W.A. Majid, M. Darroudi, T.S. Velayutham, Experimental and theoretical dielectric studies of PVDF/PZT nanocomposite thin films, *Ceramics International* 37(5) (2011) 1653-1660.
- [21] S. Janakiraman, A. Surendran, S. Ghosh, S. Anandhan, A. Venimadhav, Electroactive poly (vinylidene fluoride) fluoride separator for sodium ion battery with high coulombic efficiency, *Solid State Ionics* 292 (2016) 130-135.
- [22] L. Ruan, X. Yao, Y. Chang, L. Zhou, G. Qin, X. Zhang, Properties and Applications of the  $\beta$  Phase Poly (vinylidene fluoride), *Polymers* 10(3) (2018) 228.
- [23] J. Xing, Q.-Q. Ni, B. Deng, Q. Liu, Morphology and properties of polyphenylene sulfide (PPS)/polyvinylidene fluoride (PVDF) polymer alloys by melt blending, *Composites Science and Technology* 134 (2016) 184-190.
- [24] C. Tsonos, C. Pandis, N. Soin, D. Sakellari, E. Myrovali, S. Kriptou, A. Kanapitsas, E. Siores, Multifunctional nanocomposites of poly (vinylidene fluoride) reinforced by carbon nanotubes and magnetite nanoparticles, *Express Polymer Letters* 9(12) (2015).
- [25] K. Behera, M. Yadav, F.-C. Chiu, K.Y. Rhee, Graphene Nanoplatelet-Reinforced Poly (vinylidene fluoride)/High Density Polyethylene Blend-Based Nanocomposites with Enhanced Thermal and Electrical Properties, *Nanomaterials* 9(3) (2019) 361.
- [26] K. Jurczuk, A. Galeski, M. Mackey, A. Hiltner, E. Baer, Orientation of PVDF  $\alpha$  and  $\gamma$  crystals in nanolayered films, *Colloid and polymer science* 293(4) (2015) 1289-1297.
- [27] M.-m. Tao, F. Liu, B.-r. Ma, L.-x. Xue, Effect of solvent power on PVDF membrane polymorphism during phase inversion, *Desalination* 316 (2013) 137-145.
- [28] T.T. Van Tran, S.R. Kumar, S.J. Lue, Separation mechanisms of binary dye mixtures using a PVDF ultrafiltration membrane: Donnan effect and intermolecular interaction, *Journal of Membrane Science* 575 (2019) 38-49.
- [29] X. Cai, T. Lei, D. Sun, L. Lin, A critical analysis of the  $\alpha$ ,  $\beta$  and  $\gamma$  phases in poly (vinylidene fluoride) using FTIR, *RSC advances* 7(25) (2017) 15382-15389.
- [30] H. Ngang, B. Ooi, A. Ahmad, S. Lai, Preparation of PVDF-TiO<sub>2</sub> mixed-matrix membrane and its evaluation on dye adsorption and UV-cleaning properties, *Chemical engineering journal* 197 (2012) 359-367.
- [31] M.R. Elmarghany, A.H. El-Shazly, S. Rajabzadeh, M.S. Salem, M.A. Shouman, M.N. Sabry, H. Matsuyama, N. Nady, Triple-Layer Nanocomposite Membrane Prepared by Electrospinning Based on Modified PES with Carbon Nanotubes for Membrane Distillation Applications, *Membranes* 10(1) (2020) 15.
- [32] M.S. Salem, A.H. El-Shazly, N. Nady, M.R. Elmarghany, M.N. Sabry, PES/PVDF blend membrane and its composite with graphene nanoplates: Preparation, characterization, and water desalination via membrane distillation, *Desalin. Water Treat* 166 (2019) 9-23.
- [33] M.S.A. Salem, A.H. El-Shazly, M.R. El-Marghany, M.N. Sabry, N. Nady, Effect of adding functionalized graphene on the performance of PVDF membrane in direct contact membrane distillation, *Key Engineering Materials*, Trans Tech Publ, 2019, pp. 337-342.